IEEE Journal of Microwaves

Received 5 November 2022; revised 7 December 2022; accepted 12 December 2022; date of current version 27 December 2022.

Digital Object Identifier 10.1109/JMW.20XX.0000000

On-Wafer Vector-Network-Analyzer Measurements at mK Temperatures

E. McEntee Wei[1,2] (Graduate Student Member, IEEE), R. A. Chamberlin[1,3], N. Kilmer[1,4] (Member, IEEE), J. Kast[1,5] (Student Member, IEEE), J. A. Connors[1], D. Williams[1] (Life Fellow, IEEE)

[1]National Institute of Standards and Technology, Boulder, CO 80305 USA
[2]Department of Physics, Colorado School of Mines, Golden, CO 80401 USA
[3]Quantum Circuits, Inc., New Haven, CT 06511, USA
[4]Bold Renewables, Windsor, CO 80550, USA
[5]Department of Electrical Engineering, Colorado School of Mines, Golden, CO 80401 USA

CORRESPONDING AUTHOR: D. Williams (e-mail: dylan.williams@nist.gov).

ABSTRACT We describe a system for performing on-wafer vector-network-analyzer measurements from 100 MHz to 15 GHz at mK temperatures (*i.e.*, less than 20 mK). We first demonstrate a camera-less probe positioning system and calibrate this system at 4.4 K. We then use this positioning system to perform both on-wafer scattering-parameter calibrations and on-wafer large-signal-network-analysis calibrations at 4.4 K and mK temperatures. The scattering-parameter calibrations were based on cooled printed transmission lines while the power and electrical phase calibrations required for on-wafer large-signal network analysis calibrations were performed by transferring room temperature coaxial power and electrical phase calibrations through long attenuated coaxial lines to our cryogenic on-wafer reference plane. Finally, we perform scattering-parameter measurements of common interconnect structures and measurements of modulated-signals typical of those used to control superconducting transmon qubits commonly used in quantum-computing applications. We also demonstrate our ability to predistort the modulated signals we created, and we assess the drift and stability of our system, which we found to be on the order of a few tenths of a dB and a few degrees.

INDEX TERMS Cryogenic measurement, large-signal network analysis, on-wafer measurement, vector network analysis.

I. INTRODUCTION

We construct an on-wafer vector-network-analyzer (VNA) measurement system with commercial microwave wafer probes and a camera-less positioning system for use from 100 MHz to 15 GHz at mK temperatures[1]. We use the system to perform both scattering-parameter and large-signal network analysis calibrations followed by calibrated measurements of interconnect structures and modulated signals at mK temperatures and assess the measurement stability of the system.

Microwave scattering-parameter measurements performed at mK temperatures have proved extremely useful in the design of microwave components used for qubit control and readout. While we and others have been performing on-wafer microwave measurements at 4 K for some time [1-5], microwave measurements at mK temperatures are more challenging: signals input into the dilution refrigerators used to reach mK temperatures must be greatly attenuated to reduce noise and control thermal loading, signals exciting nonlinear circuits must be weak,

[1] We use this term to mean less than 20 mK generally, but between 8 mK and 13 mK when referring to the work we report on in this paper.

cooling power is limited, cabling is long and obtaining repeatable measurements is difficult.

The first system for performing calibrated two-port vector scattering parameters at mK temperatures was reported by Ranzani, *et al*., in [6]. Ranzani, *et al*. described a thru-reflect-line (TRL) calibration approach in coaxial transmission lines based on electromechanical coaxial switches. The switches allowed for routing signals from the VNA to coaxial calibration standards and a coaxial device under test (DUT). Ranzani, *et al*. applied their approach to the development and characterization of connectorized circuits in [7, 8] and similar approaches have been used since then by Yeh, *et al*. [9], Oates, *et al*. [10] and others [11, 12].

More recently, the claim from Google in [13] of the achievement of "Quantum Supremacy" (*i.e.*, the development of a quantum computer capable of solving problems that cannot be solved with conventional computers) has illustrated both the great potential of quantum computing and the difficulties of scaling up the size of quantum computers to perform error correction and solve larger problems. Consequently, a number of groups and companies, including Intel [14, 15], IBM [16], Honeywell [17] and Google [18, 19], have advocated for and/or are investigating applying integrated-circuit technology and interconnects to the construction of the next generation of quantum computers. See also [20-24].

In response to this emphasis on integrated circuits and integrated-circuit interconnects, Stanley, *et al*. developed the first system for performing calibrated microwave scattering-parameter measurements by embedding planar calibration artifacts and DUTs in a fixture and using an electromechanical coaxial switch to switch between the planar calibration standards and the DUT [25, 26]. Stanley, *et al*. demonstrated the first on-wafer measurements of integrated circuits at mK temperatures with this approach.

In this work, we present the next logical step in this progression, the development of an on-wafer probing system capable of stepping between planar calibration standards and DUTs, and performing calibrated scattering-parameter and large-signal vector network analysis at mK temperatures without packaging the calibration standards and DUTs in special fixtures. To accomplish this, we introduce microwave hardware similar to that used in [27] to extend the types of measurements we are able to perform to include power and electrical-phase calibrations. The result is a single-instrument on-wafer probing solution for physicists and engineers capable of making a variety of calibrated microwave frequency-domain and temporal measurements at mK temperatures.

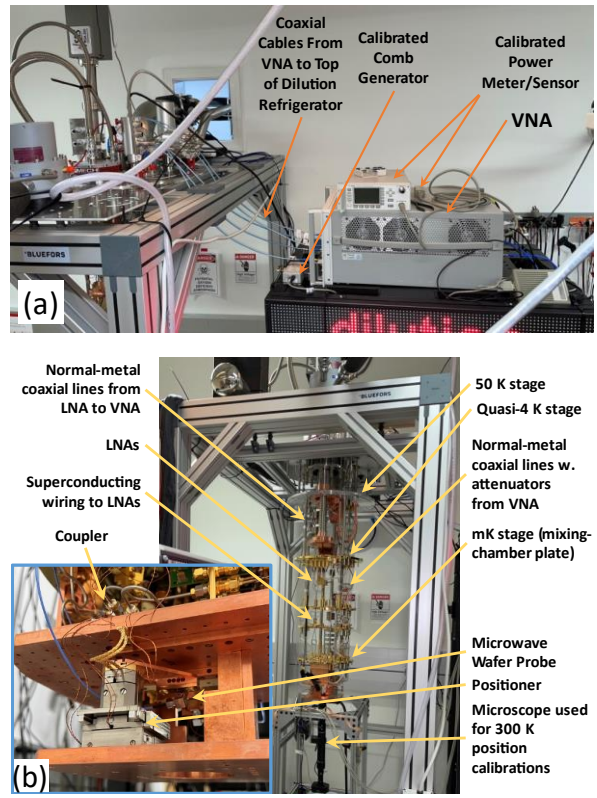

FIGURE 1. **Overview of the system. (a) The VNA and cables used to perform the scattering-parameter and modulated-signal measurements. (b) The inside of the dilution refrigerator.**

II. ON-WAFER MEASUREMENT-SYSTEM OVERVIEW

In this section we will describe the on-wafer measurement system we developed. Figure 1 shows photographs of the on-wafer measurement system, Fig. 2 shows a schematic of the microwave hardware we used, and Fig. 3 shows the layout of the printed circuit board (PCB) we used for our demonstrations.

A. PHYSICAL LAYOUT

Figure 1a contains a photograph of our Agilent N5245A VNA[2] and Fig. 1b contains a photograph of the inside of the BlueFors LD400 dilution refrigerator we used to cool the experiment. The coaxial electrical connections between the VNA and electrical equipment inside the dilution refrigerator are routed through the top of the dilution refrigerator and then thermalized at the 50 K, Quasi-4 K and mK temperature stages in the refrigerator with in-line attenuators at each stage. These attenuators also reduce microwave noise and power levels, which in turn reduces thermal loading at the mixing-chamber plate (the coldest mK stage) of the refrigerator.

[2] We use brand names only to clarify the experimental configuration. The National Institute of Standards and Technology does not endorse commercial products. Other products may work as well or better.

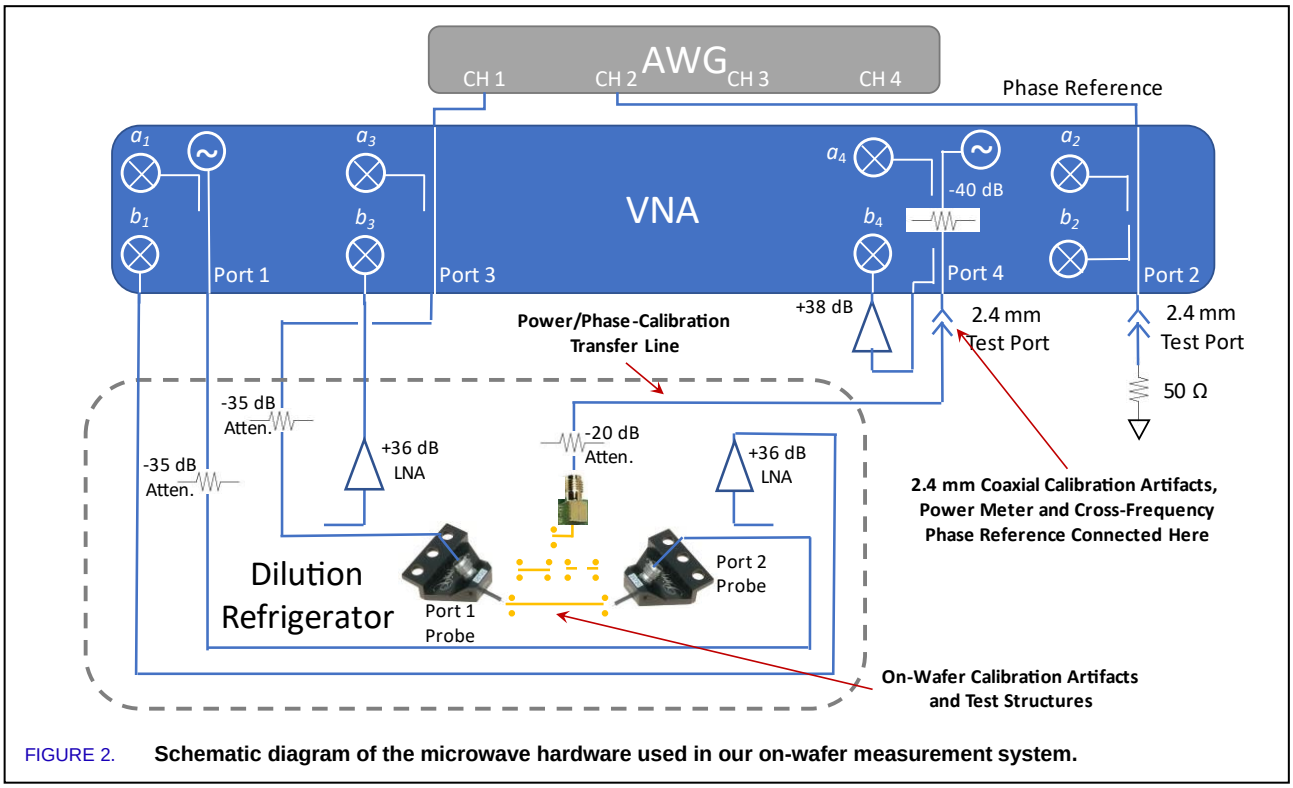

FIGURE 2. **Schematic diagram of the microwave hardware used in our on-wafer measurement system.**

We attached our experimental apparatus to the bottom of the mixing-chamber plate (see inset at bottom-left of Fig. 1b). Thus, the positioners, the 150 µm pitch brass-bodied wafer probes fabricated by GGB Industries, and PCB are all positioned below the mixing-chamber plate. The PCB, which contains all the planar calibration standards and DUTs, is mounted upside down underneath the mixing plate to improve its thermal anchoring. The probes are moved with piezoelectrically driven positioners mounted below the PCB during the performance of on-wafer calibrations and measurements.

Finally, there is a microscope and stand below the dilution refrigerator used for performing initial 300 K positioning calibrations. The microscope helps to orient the user while completing this stage of the positioning calibration. The results of this initial room-temperature positioning calibration are then used to allow for full automation of the positioning calibration performed once the positioners reach 4.4 K. This microscope and stand must be removed before the refrigerator is closed and cooled.

B. MICROWAVE HARDWARE

Figure 2 contains a sketch of the microwave components used for the scattering-parameter and modulated-signal measurements. The microwave configuration is similar to that first presented in [6] for performing coaxial scattering-parameter calibrations at mK temperatures. We targeted the frequency range 500 MHz to 14 GHz due to the preponderance of applications in that frequency range. However, hardware for extending the frequency range to 40 GHz is already commercially available.

The 35 dB attenuators in the dilution refrigerator reduce the power levels below the 14 µW cooling limit of our refrigerator and keep the electrical noise in the system to levels suitable for controlling transmon qubits without attenuating the signals more than necessary for these first experiments. The incident waves are measured by couplers in the VNA. We used two custom brass Marki Microwave 9 dB CX0477 450 MHz to 18 GHz microwave directional couplers[3] in the dilution refrigerator to separate out the weak reflected waves at the on-wafer ports of the planar DUT. The 36 dB Low Noise Factory LNF-LNC0.3_14A 300 MHz to 14 GHz low-noise amplifiers (LNAs) in the dilution refrigerator amplify the weak signals reflected from the planar DUT before they are measured by the receivers in the VNA outside of the refrigerator. This configuration increases the sensitivity of the VNA by moving key components of the VNA front end into the bottom of the dilution refrigerator.

The attenuators and the 38 dB Mini Circuits ZVA-183GX-S+ 500 MHz to 18 GHz wideband amplifier at the room-temperature coaxial port of the VNA serve to balance the power levels at this port with the power levels at the bottom of the dilution refrigerator. As discussed in Section IV, this facilitates the transfer of the power and electrical phase calibrations from the VNA's room-temperature

[3] While this part number is not listed in the Marki catalog it is now available from Marki as a special order.

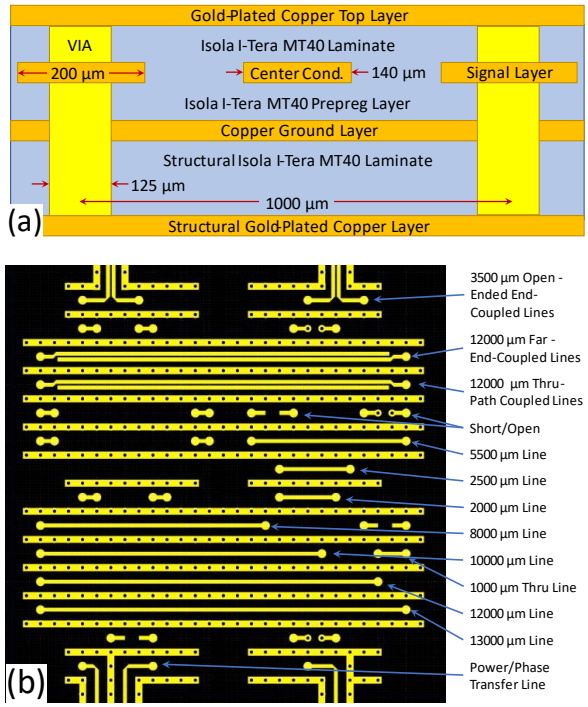

FIGURE 3. **The cross section (a) and signal layer (b) of the PCB we used in these experiments.**

coaxial port to the cold on-wafer reference planes on the PCB in the refrigerator.

Finally, we optimized our experiment for the measurement of scattering parameters and the moderate signal levels that are commonly used to control transmon qubits. Keeping the attenuation and gain at roughly the 35 dB level helped keep drift low. However, when working with qubits, the sensitivity of the entire setup must often be further increased by increasing the attenuation used to supply energy to the on-wafer reference plane to about 70 dB and adding additional room-temperature gain blocks in the reflected-wave paths. Of course, in our case, increasing attenuation and gain at the room-temperature coaxial port would also be necessary. When increasing the sensitivity of the VNA front end in this way, we expect that it would be best to leave the attenuation in the power/phase-calibration transfer cable fixed at about 20 dB to keep the signal-to-noise ratio high during the transfer of the power and phase calibrations from room temperature to mK temperatures, as this line is only used during the calibration and does not inject any noise into sensitive components during DUT measurements.

C. PRINTED CIRCUIT BOARD

We used striplines on a circuit board manufactured by Rush PCB in a four-metal-layer fabrication process in our experiments. We chose stripline in large part because it is commonly used in interconnects of interest for quantum-computing applications [21-23, 28, 29].

The PCB had a 35 µm thick patterned gold-plated-copper top layer, a 152 µm thick Isola I-Tera MT40 laminate, a 17.5 µm thick patterned copper signal layer, a 152 µm thick Isola I-Tera MT40 prepreg layer and a final 17.5 µm thick copper ground layer, as shown in Fig. 3a. This stackup was backed by an additional 762 µm thick Isola I-Tera MT40 laminate backed by a final gold-plated 35 µm thick copper metal layer for structural support. The Isola I-Tera MT40 laminate material has a nominal relative dielectric constant of 3.45.

Figure 3b shows the signal layer of the PCB and the placement of the planar calibration artifacts and DUTs we report on here. We used the shorts, opens and lines as calibration artifacts and the coupled lines as DUTs. The striplines, which had a 140 µm wide center conductor and a nominal characteristic impedance of 50 Ω, were fabricated on the signal layer sandwiched between the top copper layer and the copper ground layer. We used rows of 125 µm diameter vias spaced 500 µm apart and connected by 200 µm wide "ground rails" on the signal layer spaced 500 µm from the center of the stripline center conductor to stitch the top metal layer and metal ground layer together. We also used 150 µm diameter vias to connect signal pads on the top copper layer to the round landing pads at the ends of the center conductors of the striplines on the signal layer shown in Fig. 3.

III. POSITIONING CALIBRATION

We used stacks of ANPx341/RES+/LT/HV and ANPz102/RES+/LT/HV nano-positioners with piezoelectric drives manufactured by attocube systems AG to position our probes and bring them into contact with the PCB we used for this demonstration. These positioners are designed for low-temperature operation and come equipped with resistive position-sensing encoders to allow for both open-loop and closed-loop positioning control.

We performed a series of room-temperature experiments to understand how to best operate these positioners. These experiments indicated that it was best to always approach our target utilizing the controller's closed-loop mode in the forward direction after incorporating a 300 µm anti-backlash movement, and to turn off the controller's closed-loop mode immediately after the positioner arrived at its destination. We also compared using 1) the ideal target position we set for the closed-loop positioning system, which continuously monitors the resistive position sensor as the positioner approaches the target, and 2) the position we measure after the positioner arrives at its destination and we turn off the closed-loop control. We found that the ideal target position we set for the closed-loop positioning system to be more repeatable in room-temperature experiments. We also observed that the usual 1 µm to 2 µm discrepancies between the two methods at room temperature we observed generally increased to 5 µm to 20 µm at cryogenic temperatures. We believe this increase in the discrepancy is in large part due to adjustments of the operating parameters such as the sensing voltage and drive frequency and voltage required to control the positioners at cold temperatures, which were balanced

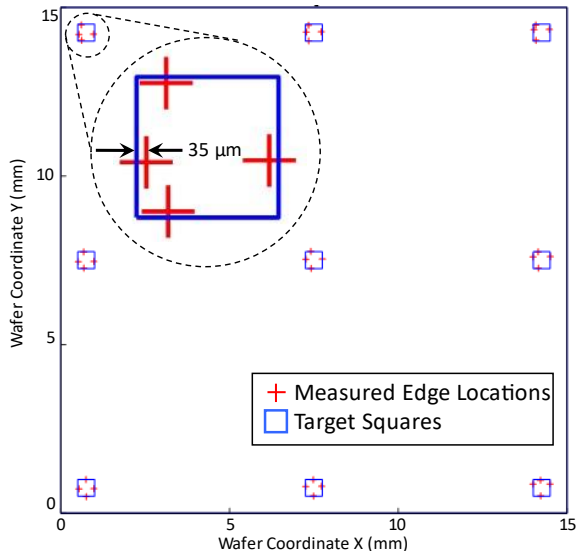

FIGURE 4. **Calculated positions of detected edges compared to fitted positions of the alignment squares printed on the top-level metal of the PCB.[4]**

for performance while minimizing heat dissipation. It is possible that these positional discrepancies could be reduced at cryogenic temperatures by further optimization of these operating parameters.

Based on these experiments, we used the ideal target position we set for the closed-loop positioning system as our best estimate of the positioner's final location. We also repeated any movements for which the difference between the target and final measured position exceeded 30 µm.

We also developed a calibration procedure to relate the positions measured by the resistive sensors to actual positions on the circuit board. We included nine 500 µm by 500 µm positioning squares etched in the top-level metal in our design for this purpose. We then developed a positioning calibration based on sensing DC electrical contact to first find the height of the conducting surface on the PCB near each square, and then to step along the conducting surface and locate the four edges of the nearby square to determine the location of the square's center.

To make finding the alignment squares robust when the microscope was not available and to better account for differential thermal contraction in the measurements system when cooling to 4.4 K, we applied this positioning calibration procedure twice. First, we performed the calibration procedure at room temperature, where we could set starting positions for the algorithm with the aid of the auxiliary microscope shown in Fig. 1a. Then, we removed the auxiliary microscope and cooled the refrigerator down to 4.4 K, where we still retain sufficient cooling power to consistently drive the positioners while only raising the mixing-chamber plate by about 100 mK, and repeated the calibration using just four of the nine calibration squares without the aid of the microscope. Here we relied on our room-temperature calibration to set starting points for the algorithm when performing the calibration at 4.4 K.

Figure 4 shows the 36 edge positions we detected as red crosses during one of the room-temperature positioning calibrations we performed.[4] The figure also shows the positions of the nine calibration squares in blue. If the resistive position sensors were completely accurate, the detected edge positions would all lie on the edges of the nine calibration squares.

Because the fit is highly overdetermined, we can estimate the accuracy of this positioning approach from differences between the measured and fitted edge locations. The largest deviation of a detected edge from the fitted calibration squares is shown in the expanded view in the upper left of Fig. 4. In this case, we found the standard deviation of our x-y placement errors to be about 20 µm and the worst-case placement error to be 35 µm (shown in the inset of Fig. 4). We found the standard deviation of the z placement errors to be about 9 µm with a worst-case placement error of 13.6 µm.

The results at 4.4 K were similar. Determining the accuracy of our positioning calibration at mK temperatures required too many probe movements at the greatly reduced cooling powers available at these temperatures to be practical. However, additional expansion or contraction when the temperature is reduced from 4.4 K to mK temperatures is small [30] and we did not have any difficulty making good electrical contact to the PCB, indicating that the positioning calibration was not significantly degraded during the final cooling step to mK temperatures.

This positioning error is adequate for the demonstration we present here using probes with a 150 µm pitch. However, our positioning accuracy would have to be improved when performing higher-frequency measurements with tighter probe pitches and smaller contact pads.

IV. MICROWAVE CALIBRATION

We can perform either one-port or two-port microwave scattering-parameter calibrations with the microwave hardware configuration on ports 1 and 3 of the VNA shown in Fig. 2 at the cooled on-wafer reference planes without any modification of standard scattering-parameter calibration algorithms. However, to facilitate the performance of large-signal network analysis, we do not measure raw scattering parameters. Rather, we measure raw "wave parameters", as opposed to calculating uncorrected scattering parameters immediately from their ratios [31, 32]. That is, we measure the complex amplitudes of the forward and backward waves at each port and develop calibrations that map raw measured wave

[4] The data plotted in Figs. 4-11 can be accessed at https://doi.org/10.18434/mds2-2824.

parameters directly into calibrated complex amplitudes of the forward and backward "impedance-corrected" waves [33, 34] before taking ratios and calculating scattering parameters. Working with the wave parameters directly preserves information lost when scattering parameters are formed from the ratios of the wave parameters. This, in turn, allows us to perform the power and cross-frequency phase calibrations that are essential to large-signal network analysis and access the suite of additional measurements that large-signal network analysis enables [35]. We performed the calibrations in an automated software suite called the NIST Microwave Uncertainty Framework (MUF) [36]. This suite not only allows automation, but also supports the evaluation of uncertainty distributions and their correlations.

The high attenuation and amplification needed to get signals into and out of the refrigerator prevent use of traditional 2-tier calibration strategies to transfer power and electrical phase calibrations to the cooled reference planes in the refrigerator. Thus, we use port 4 of the VNA as a coaxial room-temperature port to accommodate large-signal VNA calibrations with additional power and electrical phase calibrations. This allows us to first perform either two-port or three-port wave-parameter calibrations with either one or two cooled on-wafer reference planes, respectively, and one room temperature port at port 4 of the VNA.

We then augment these mixed-temperature two-port or three-port calibrations with additional power and electrical-phase calibrations at the coaxial room-temperature port 4 of the VNA. Since the multiport scattering-parameter calibration captures the power and phase relationships between all the ports, once we add the power and electrical-phase calibrations they can be extended to the entire multiport calibration in a single step [31, 37]. This effectively leverages our knowledge of the multiport scattering-parameter calibration model to transfer our room-temperature power and electrical-phase calibrations to the cooled on-wafer reference planes in the dilution refrigerator.

At the room-temperature port we used 2.4 mm coaxial calibration standards from a Keysight 85056A calibration kit, a calibrated Keysight 8487A 2.4 mm power sensor and E4418B EPM Series Power Meter and a NIST-calibrated [38] Keysight N10149 comb generator that serves as an electrical-phase calibration artifact. During the phase calibration with the NIST-calibrated comb generator, we used a Keysight M8195A 65 GSa/s arbitrary waveform generator (AWG) to provide a phase reference (*i.e.* synchronization signal) for the VNA from its second channel. Later, we used the AWG to generate a modulated signal on its first channel while providing the same phase reference on its second channel to the VNA for synchronization purposes. Finally, we used the MUF to perform these calibrations, which was specifically designed to support both scattering-parameter calibrations and large-signal network analysis.

However, none of this could have been done without the use of the additional "Power/Phase Calibration Transfer Line" highlighted in Fig. 2. This transfer line allowed us to "stitch together" the room-temperature and cooled on-wafer calibrations with a reciprocal "unknown" thru standard [39] with the MUF, which supports the use of reciprocal standards as a standard part of its multiport calibration routines. While the work of [39] was based on short-open-load-thru calibrations, it can be used to stitch together any two complete scattering-parameter calibrations (two one-port short-open-load calibrations in [39]). These reciprocal standards take advantage of the fact that stitching complete calibrations together can be performed just with the knowledge that the forward and reverse transmission coefficients are guaranteed equal by the Lorentz reciprocity theorem (see Sections 2.12 and 4.7 of [40]). That is, the actual scattering parameters of the reciprocal standards does not need to be known, just the fact that the forward and reverse transmission coefficients are equal [39], to stitch the calibrations together. Using this, the reciprocal standard acts to balance the forward and reverse transmission though the reciprocal connection between the two calibrations. The ability to stitch together calibrations in this way is a standard part of the MUF.

Using the transfer line as a reciprocal thru requires knowing its electrical length within 90 degrees to eliminate phase ambiguities in the microwave calibration. With this in mind, we first measured the scattering parameters of the transfer line at room temperature and cascaded them with a model for the electrical length of a short section of coaxial line, a connectorized transition from this short coaxial line to a stripline on the PCB and a short section of the stripline leading to the on-wafer reference plane. (This model was based on a one-port measurement of the reflection coefficient at the input to the short coaxial line and models of the structures on the PCB to correctly account for the position of the on-wafer reference plane in the stripline.) This gave us a good estimate of the electrical length of the complete path through the transfer line to the on-wafer reference plane at room temperature.

Finally, after performing the calibrations with the on-wafer ports at 4.4 K, we adjusted the electrical length in our models slightly until we were able to eliminate all the electrical phase ambiguities in the calibration. This allowed us to then fine-tune the model of the cooled transfer line until it matched the measured phase of the cooled transfer line over the entire measurement range with only a slight additional adjustment to the room-temperature model. We found that this fine-tuned model for the cooled transfer line could be re-used later without further modification when we warmed up and cooled down the system to resolve phase ambiguities in the mixed room-temperature coaxial and the 4.4 K and mK on-wafer calibrations.

This calibration approach not only allows us to transfer the power and electrical phase calibrations performed at room temperature to the cooled on-wafer ports, but also to measure the scattering parameters of any interconnect

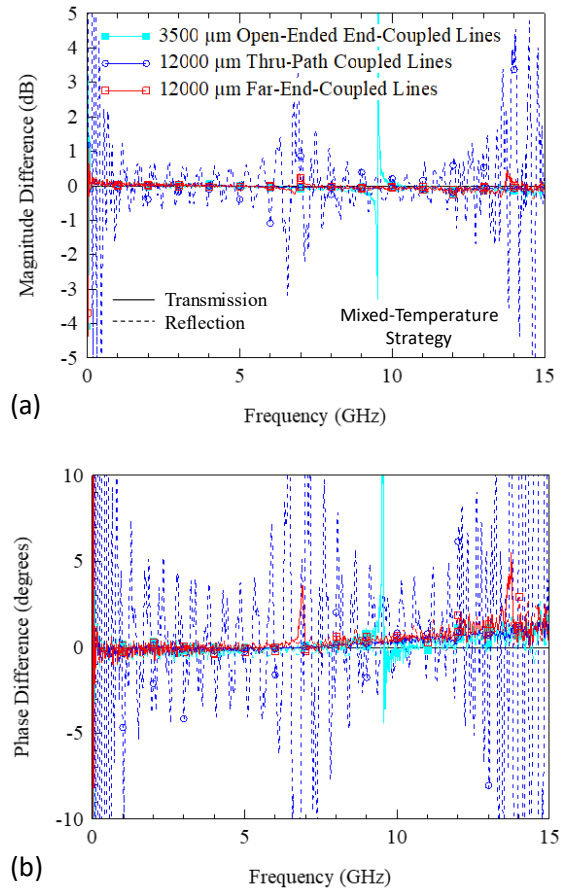

FIGURE 5. **Differences in the (a) magnitude and (b) phase of mK scattering-parameter measurements corrected with a 4.4 K calibration (*i.e.* performed with the mixed-temperature strategy) and the 4.4 K reference measurements.** [4]

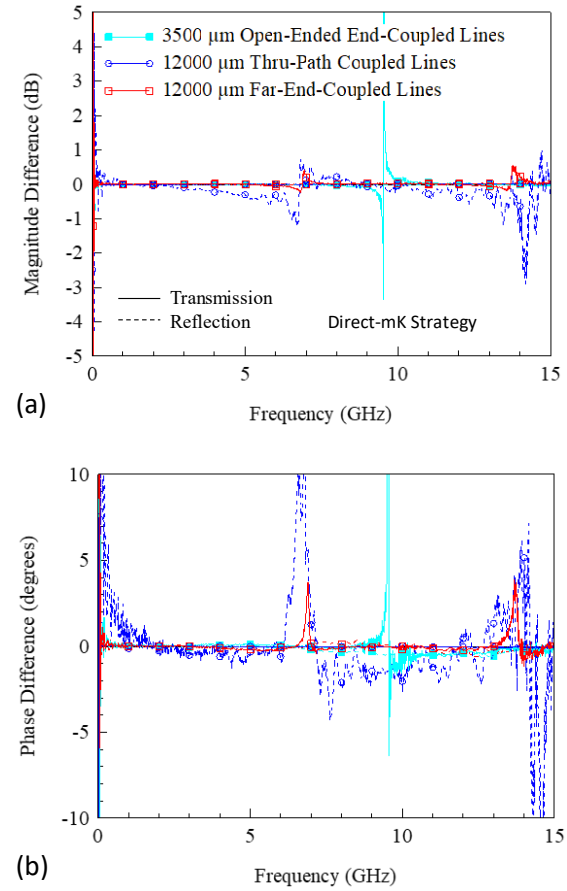

FIGURE 6. **Differences in the (a) magnitude and (b) phase of mK scattering-parameter measurements corrected with a mK calibrations (*i.e.* performed with the direct-mK strategy) and the 4.4 K reference measurements. Peak differences tend to occur near nulls in the magnitude of the quantity being plotted.** [4]

between the VNA's coaxial room-temperature port and the VNA's mK on-wafer reference planes. We also demonstrate the use of these power and electrical phase calibrations to measure and pre-distort a modulated signal at mK temperatures later in this paper.

V. MEASUREMENTS AND STABILITY

The energy required to move the positioners and probes at mK temperatures quickly heats the mixing-chamber plate and can easily exceed the capacity of the dilution refrigerator to maintain normal helium circulation by boiling off the helium mix too quickly, thereby requiring the user to recollect and recondense the helium to return to normal helium circulation. To address this, we developed an approach for positioning the probes at mK temperatures by limiting motions to smaller increments than we used a 4.4 K and allowing the dilution refrigerator to cool between these steps. However, this approach required roughly 8 hours on average to move the probes between devices, potentially increasing measurement error due to drift in the system.

Calibrating at 4.4 K and then measuring DUTs at mK temperature greatly reduces the number of movements required at mK temperatures but risks the introduction of additional measurement error due to using a scattering-parameter calibration performed while the system is at one temperature to measure the DUT while the system is at another temperature.

In this section we first compare scattering-parameter measurement errors and drift of the relatively quick "mixed-temperature" strategy, in which we calibrate at 4.4 K and then measure DUTs at mK temperatures, to the slower "direct-mK" strategy, in which we both calibrate and perform DUT measurements at mK temperatures. Then we present the best calibrated scattering-parameter measurements at mK temperatures we performed. Finally, we present calibrations and measurements for large-signal network analysis we performed in a separate experiment.

A. SCATTERING-PARAMETER CALIBRATION AND MEASUREMENT STABILITY

To compare our mixed-temperature and direct-mK calibration and measurement strategies, we first calibrated our system at 4.4 K and measured our coupled-line DUTs at 4.4 K. We then used these measurements, which we could both perform quickly and without changing the system temperature, as reference measurements for the DUTs. We chose this approach because the DUTs, which were constructed entirely of normal metals, should be fairly insensitive to the small change between 4.4 K and mK measurement temperatures.

Figures 5 and 6 compare measurements of our coupled-line DUTs, the "3500 µm Open-Ended End-Coupled Lines",[5] the "12000 µm Far-End-Coupled Lines" and the "12000 µm Thru-path Coupled Lines", (see Fig. 3). These DUTs were measured with the relatively quick mixed-temperature strategy and the slower direct-mK strategy to our 4.4 K reference measurements. Throughout, we used thru-reflect-line calibrations [41-43] based on the 13000 µm, 5500 µm, 2500 µm striplines, the 1000 µm thru line, and the short fabricated on our PCB (see Fig. 3).

This, and the other calibrations we used in this study, move the calibration reference plane to the center of the 1000 µm thru line, removing the impact of the contact pads, contact-pad via and a 500 µm section of stripline from the measurements. To determine the characteristic impedance of the striplines, we assumed that the conductance per unit length of line was negligible and the capacitance per unit length of the transmission line was constant [42, 43]. Then we estimated the capacitance per unit length of line from the manufacturers data for the dielectric constant of the materials and the stripline geometry with the Keysight Advanced Design System's Linecalc stripline calculator. This was sufficient to apply the approach of [42] to determine the characteristic impedance of the line and set the reference impedance of the calibrations to 50 Ω.

After considering the differences in the scale of Figs. 5 and 6, the figures make it clear that the error in the direct-mK strategy shown in Fig. 6 is significantly lower than the error of the mixed-temperature strategy shown in Fig. 5, despite the greater measurement time involved. Figure 6 also indicates that the measurement repeatability of our system is on the order of a few tenths of a dB in magnitude and a few degrees in phase when performed with the direct-mK strategy, despite the long cables in the measurement system.

Finally, we note that the ripples we observe in the reflection measurements performed with the mixed-temperature strategy were consistent with an additional additive error in the reflection coefficient of roughly 0.06 in the system that adds constructively and destructively with a period of roughly 500 MHz. This indicates a single source of error in the system that, with study, we may be able to identify and eliminate. We are also investigating other approaches to shortening measurement time while maintaining accuracy, including reducing the energy dissipation in the positioners, which would reduce cooling times, and improving the thermal conductivity of the positioners, which become superconducting at mK temperatures, raising their thermal impedance and impeding heat removal.

B. DIRECT-mK SCATTERING-PARAMETER MEASUREMENTS

Figures 7, 8 and 9 plot the magnitudes and phases of our coupled-line DUTs measured with the direct-mK strategy (*i.e.*, both calibration and DUT measurements performed at mK temperatures). The plots include the reflection coefficients at each port of the DUTs and both the forward and reverse transmission coefficients of each of the DUTs we measured. The measurements, which were performed

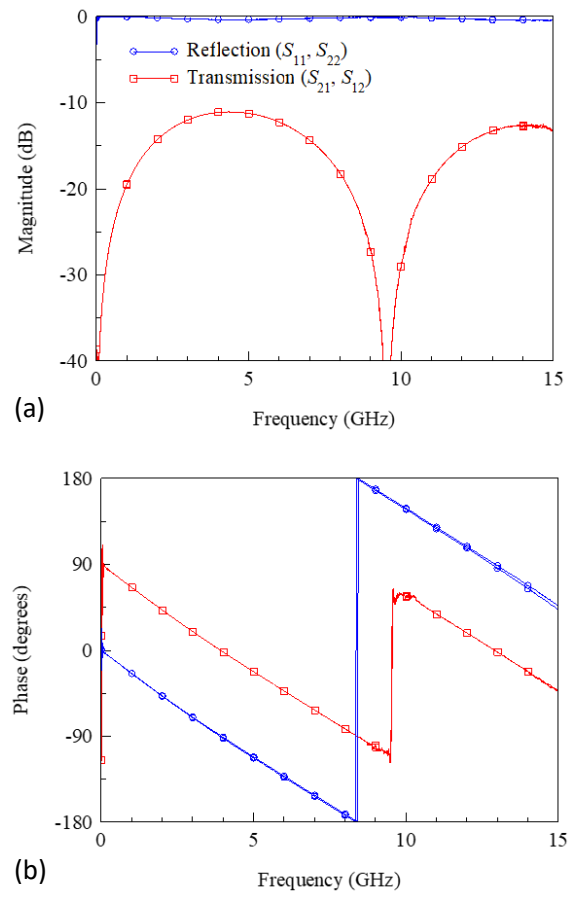

FIGURE 7. **The magnitude (a) and phase (b) of the scattering parameters of the 3500 µm Open-Ended End-Coupled Lines (see Fig. 3) performed with the direct-mK strategy.** [4]

[5] The coupled lines are terminated outside of the view shown in the figure by open contact pads originally intended for wirebonds.

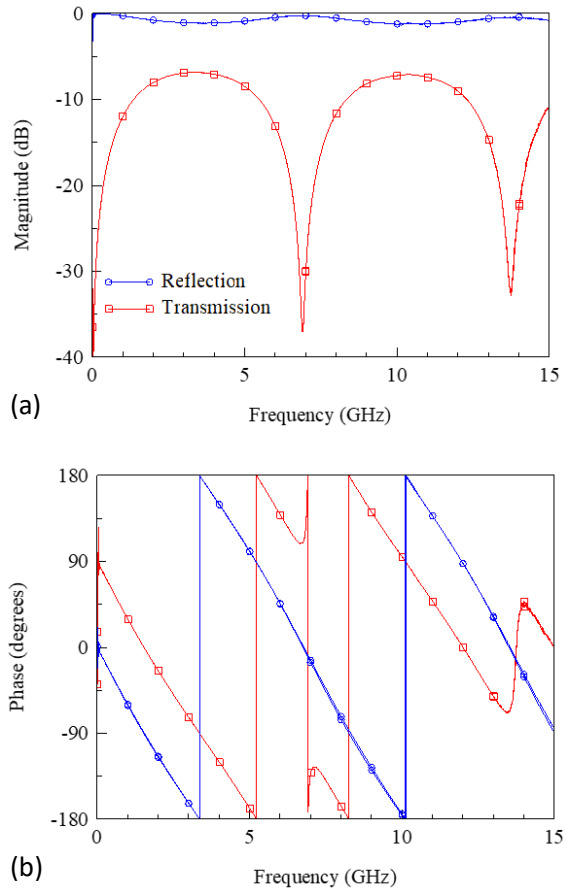

FIGURE 8. **The magnitude (a) and phase (b) of the scattering parameters of the 12000 μm Far-End-Coupled Lines (see Fig. 3) performed with the direct-mK strategy.** [4]

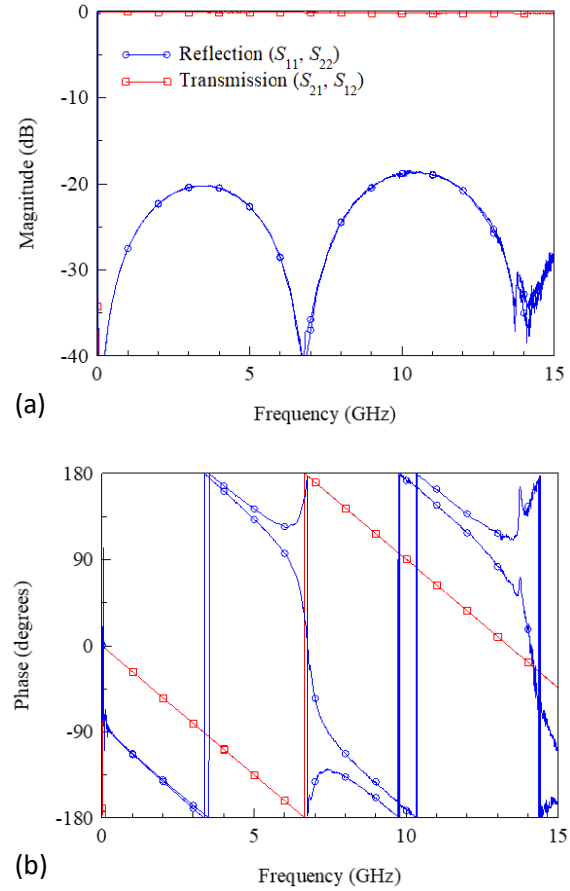

FIGURE 9. **The magnitude (a) and phase (b) of the scattering parameters of the 12000 μm Thru-Path Coupled Lines (see Fig. 3) performed with the direct-mK strategy.** [4]

on a 10 MHz grid, are generally smooth and well behaved. The differences between the measurements on different ports are generally small, although we do see more significant differences in the phases of the two relatively low-magnitude reflection coefficients in Fig. 9.

C. MODULATED-SIGNAL MEASUREMENTS

We performed a large-signal calibration in our system based on one-port calibration artifacts and the Power/Phase Transfer Line (see Figs. 2 and 3) with the goal of demonstrating the use of this transfer line in the system. We used the mixed-temperature strategy as obtaining the most accurate calibration was not a requirement for this demonstration.

At the cooled on-wafer plane, we used the short and the open calibration artifacts and, to compensate for our lack of resistive loads on the PCB, we used all the lines available to us in an offset-open configuration as modeled loads in the calibration. At the room-temperature coaxial port of the VNA we used the 2.4 mm coaxial short, open and load standards from our coaxial calibration kit, and the 2.4 mm power meter and comb generator to perform the power and cross-frequency phase calibrations.

After performing the calibration, we used the AWG to generate the 100 ns train of 10 ns raised-cosine pulses shown in Fig. 10a. Each of the ten pulses had a 6 GHz carrier frequency but a different magnitude and/or phase. Figure 10b shows the corresponding 101-tone modulated signal in the frequency domain, which had a 10 MHz tone spacing and a repetition rate of 100 ns. This modulation is typical of those used to control transmon qubits at the cooled on-wafer reference plane [18, 19, 24]. We then used our VNA to measure this signal using the approach discussed in [27] and applied an experimental predistortion algorithm to the modulated signal to try to improve its quality.

To better understand the predistortion process and our measurement system, we estimated the dynamic range of our measurement system to be approximately 105 dB at 6 GHz. Thus, we see that the LNAs in the system preserve the VNA's inherent dynamic range. We performed the

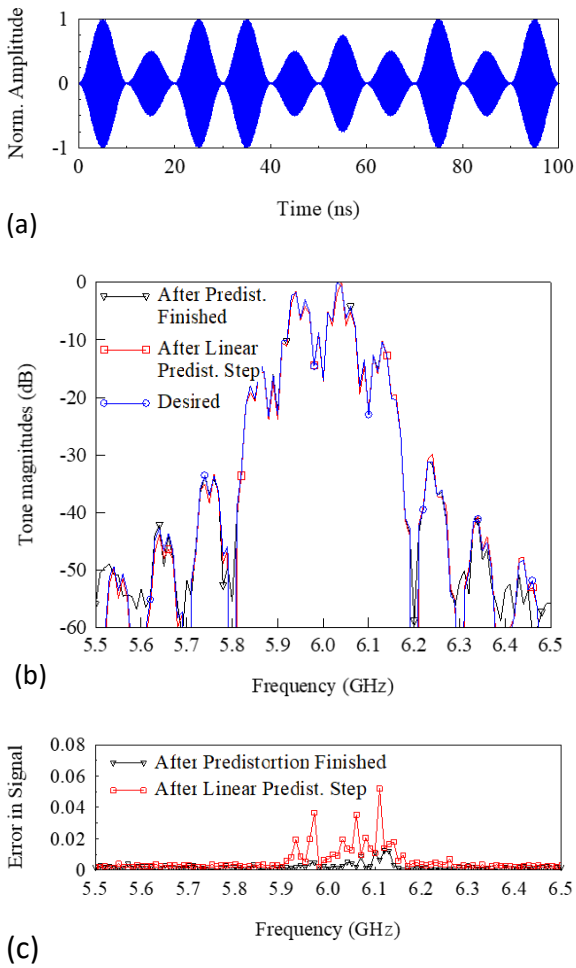

FIGURE 10. **Desired and predistorted waveforms. Measurements performed at mK temperatures. (a) The desired raised-cosine pulse train. (b) The magnitude of the desired waveform (marked with blue circles), the measured waveform after the initial linear predistortion step (marked with red squares) and the measured waveform after the predistortion algorithm has finished its final iteration (marked with black triangles). (c) Error in the signal after initial linear predistortion step and after final predistortion iteration.** [4]

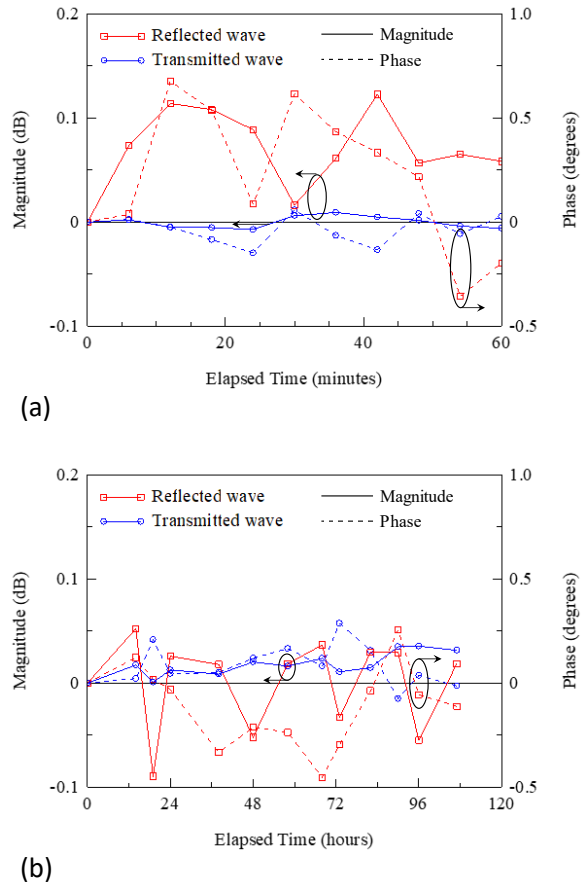

FIGURE 11. **The measured magnitude and phase drift of the 6.04 GHz tone of the modulated signal we measured at mK temperatures. (a) One-hour time scale. (b) 100-hour time scale.** [4]

estimate by comparing the point at which the LNAs and VNA receivers enter compression to the system's noise floor. The LNAs had a compression point of about -10 dBm and VNA receivers had a recommended maximum signal level of -17 dBm, so we assumed a -17 dBm maximum operating power at the VNA receivers for the overall system. We also observed a roughly -120 dBm to -125 dBm noise level at the VNA receivers when using a 1 Hz VNA intermediate-frequency bandwidth after the signal from the AWG had been turned off.

The goal of the predistortion algorithm is to optimally use the available dynamic range of the AWG while replicating as well as possible the desired modulated signal to within an arbitrary scaling factor. The experimental predistortion algorithm first measures the transfer function from the digital domain through the AWG and measurement system to the cooled on-wafer reference plane by measuring a Schroeder multisine [44] with a uniform power distribution over its 1 GHz bandwidth. The algorithm begins with a single initial linear predistortion step based on this transfer function. Figure 10b compares the desired waveform (marked with blue circles in the figure) to the signal after applying this single initial linear predistortion step (marked with red squares in the figure). If the system were completely linear, this first linear step would have reproduced the desired waveform and no further iteration would have improved the result.

The predistortion algorithm then proceeds to iteratively step towards a better solution that accounts for nonlinearity in the system. The black curve marked with triangles in Fig. 10b shows the predistorted result after the algorithm has finished this set of additional predistortion iterations. The strongest tone in this final predistorted signal was located at 6.03 GHz and had a measured power of -85.2 dBm.

Figure 10c shows the total error (*i.e*. root-mean-square of the real and imaginary parts of the error) in each tone of the initial linear predistortion step and the error in the final predistorted signal normalized to the amplitude of the maximum tone of the signal. An improvement in signal quality of the final predistorted signal (black with triangles) over that achieved with the initial predistortion step is evident for the tones at the highest power levels, although there was also improvement for tones with lower power levels. We are working on addressing nonlinear behavior in the measurement system and avoiding intermodulation products created in the VNA, which may have reduced the accuracy of our predistortion algorithm, as well as slowed the predistortion process.

Finally, Fig. 11 examines the drift we observed at the 6.04 GHz tone of our modulated signal, which we selected because it had an easily measured signal level, on a 1 hour and a 100-hour time scale. We switched between scattering-parameter and wave-parameter measurements roughly every six minutes when taking the short-term drift measurements plotted in Fig. 11a and every six hours when taking the long-term drift measurements plotted in Fig. 11b.

The drift of the signal transmitted from the AWG to the mK-temperature on-wafer reference plane and then through the transfer line back to the VNAs room-temperature port is labeled with blue circles in Fig. 11. The drift of the lower-power signal reflected from the mK-temperature on-wafer reference plane back through the cooled coupler and cooled LNA to the room-temperature receiver at the VNA is labeled with red squares in the figure. The drift was on the order of ±0.1 dB and ±0.5 degrees over both time scales for these signals, quite low given the several meters of cable in the measurement system. Finally, it is possible that the slightly larger drift in the short-term drift experiment shown in Fig. 11a has some significance, but we have not collected enough measurements to say anything definitive.

VI. CONCLUSION

Due to the difficulty of acquiring microwave measurements at mK temperatures, a single system for performing many different types of microwave measurements simultaneously at mK temperatures would be very attractive. This work enables a host of accurate on-wafer microwave measurements at mK temperatures with our on-wafer approach. These include:

1. The scattering-parameter and modulated-signal measurements discussed here. These modulated-signal measurements can be extended to narrower tone spacings and arbitrary frequency grids, as long as they lie in the bandwidth of measurement system [27, 45].
2. The characterization of nonlinear superconducting circuits, including the ability to capture harmonics and intermodulation products, as well as their embedding impedances, as discussed in [46]. This enables the exploration of both the temporal and frequency-domain microwave behavior of nonlinear and other devices. This capability is made possible by the power and electrical phase calibrations that enable the application of Fourier transforms to signals measured by the VNA.
3. The characterization of both on-wafer interconnects and interconnects between room-temperature coaxial reference planes to mK on-wafer reference planes.
4. Mismatch-corrected on-wafer power measurements. This could lead to better comparisons of room-temperature microwave power measurements with those performed by more sensitive and accurate cryogenic power sensors. This also sets the stage for tying microwave power measurements more closely to microwave noise-power measurements.

ACKNOWLEDGMENT

We owe a great debt of gratitude to our colleagues Drs. Peter Hopkins, Jose Aumentado, Manuel C. Castellanos Beltran and Adam Sirois for assisting us in the purchase and operation of our dilution refrigerator and for consulting with us on working at cryogenic and mK temperatures. We also are grateful to Dr. Chris Long for discussing our microwave calibration approach and offering suggestions for improvement. In addition, we extend our thanks to Professor Serena Eley for discussions on optimizing the operation of our probe assembly both at room and mK temperatures.

REFERENCES

[1] A. S. Boaventura *et al.*, "Cryogenic Calibration of a Quantum-based Radio Frequency Source," presented at the ARFTG Microw. Meas. Conf., Los Angeles, CA, 2020.

[2] A. S. Boaventura *et al.*, "Microwave Characterization of Superconducting Circuits," in *Applied Superconductivity Conf.*, November 2018.

[3] A. S. Boaventura, D. F. Williams, G. Avolio, and P. D. Hale, "Traceable Characterization of Broadband Pulse wavefroms Suitable for Cryogenic Josephson Voltage Applications," in *IEEE Int. Microw. Symp.*, 10-15 June 2018, pp. 1176-1179, doi: 10.1109/MWSYM.2018.8439425.

[4] A. S. Boaventura *et al.*, "Microwave Modeling and Characterization of Superconductive Circuits for Quantum Voltage Standard Applications at 4 K," *IEEE Transactions on Applied Superconductivity*, vol. 30, no. 2, pp. 1-7, 2020, doi: 10.1109/TASC.2019.2963403.

[5] J. A. Brevik *et al.*, "Cryogenic Calibration of the RF Josephson Arbitrary Waveform Synthesizer," in *2020 Conference on Precision Electromagnetic Measurements (CPEM)*, 24-28 Aug. 2020 2020, pp. 1-2, doi: 10.1109/CPEM49742.2020.9191746.

[6] L. Ranzani, L. Spietz, Z. Popovic, and J. Aumentado, "Two-port microwave calibration at millikelvin temperatures," *Review of Scientific Instruments*, vol. 84, no. 3, p. 034704, 2013/03/01 2013, doi: 10.1063/1.4794910.

[7] L. Ranzani *et al.*, "Wideband Isolation by Frequency Conversion in a Josephson-Junction Transmission Line," *Physical Review Applied*,

vol. 8, no. 5, p. 054035, 11/17/ 2017, doi: 10.1103/PhysRevApplied.8.054035.

[8] L. Ranzani, L. Spietz, and J. Aumentado, "Broadband calibrated scattering parameters characterization of a superconducting quantum interference device amplifier," *Applied Physics Letters*, vol. 103, no. 2, p. 022601, 2013/07/08 2013, doi: 10.1063/1.4813549.

[9] J.-H. Yeh and S. M. Anlage, "In situ broadband cryogenic calibration for two-port superconducting microwave resonators," *Review of Scientific Instruments*, vol. 84, no. 3, p. 034706, 2013/03/01 2013, doi: 10.1063/1.4797461.

[10] D. E. Oates, R. L. Slattery, and D. J. Hover, "Cryogenic test fixture for two-port calibration at 4.2 K and above," in *2017 89th ARFTG Microwave Measurement Conference (ARFTG)*, 9-9 June 2017 2017, pp. 1-4, doi: 10.1109/ARFTG.2017.8000842.

[11] C. R. H. McRae, "Measurement Techniques for Superconducting Microwave Resonators Towards Quantum Device Applications," in *2022 IEEE/MTT-S International Microwave Symposium - IMS 2022*, 19-24 June 2022 2022, pp. 230-232, doi: 10.1109/IMS37962.2022.9865517.

[12] S. Simbierowicz, V. Y. Monarkha, S. Singh, N. Messaoudi, P. Krantz, and R. E. Lake, "Microwave calibration of qubit drive line components at millikelvin temperatures," *Applied Physics Letters*, vol. 120, no. 5, p. 054004, 2022/01/31 2022, doi: 10.1063/5.0081861.

[13] F. Arute *et al.*, "Quantum supremacy using a programmable superconducting processor," *Nature*, vol. 574, no. 7779, pp. 505-510, 2019/10/01 2019, doi: 10.1038/s41586-019-1666-5.

[14] Intel. "Intel Introduces 'Horse Ridge' to Enable Commercially Viable Quantum Computers." https://newsroom.intel.com/news/intel-introduces-horse-ridge-enable-commercially-viable-quantum-computers/#gs.3imy1b (accessed.

[15] J. Clarke. "What It Will Take to Make Quantum Computers Practical." https://newsroom.intel.com/editorials/what-it-will-take-make-quantum-computers-practical/#gs.iv30glewsroom (accessed 2022).

[16] IBM. "Quantum Starts Here." https://www.ibm.com/quantum-computing/?p1=Search&p4=437000503859647 05&p5=e&cm_mmc=Search_Google-_-1S_1S-_-WW_NA-_-ibm%20quantum%20computing_e&cm_mmca7=71700000061253574&cm_mmca8=aud-384354108630%3Akwd-318569543695&cm_mmca9=EAIaIQobChMI2Kq3yqvr6AIVsYFaBR0PBQb5EAAYASAAEgJdmfD_BwE&cm_mmca10=427831691189&cm_mmca11=e&gclid=EAIaIQobChMI2Kq3yqvr6AIVsYFaBR0PBQb5EAAYASAAEgJdmfD_BwE&gclsrc=aw.ds (accessed 2020).

[17] J. M. Pino *et al.*, "Demonstration of the QCCD trapped-ion quantum computer architecture," *Quantum Physics*, 2020, doi: arxiv 2003.01293.

[18] J. C. Bardin *et al.*, "Design and Characterization of a 28-nm Bulk-CMOS Cryogenic Quantum Controller Dissipating Less Than 2 mW at 3 K," *IEEE Journal of Solid-State Circuits*, vol. 54, no. 11, pp. 3043-3060, 2019, doi: 10.1109/JSSC.2019.2937234.

[19] J. C. Bardin *et al.*, "A 28nm Bulk-CMOS 4-to-8GHz ¡2mW Cryogenic Pulse Modulator for Scalable Quantum Computing," in *2019 IEEE International Solid- State Circuits Conference - (ISSCC)*, 17-21 Feb. 2019 2019, pp. 456-458, doi: 10.1109/ISSCC.2019.8662480.

[20] D. J. Reilly, "Engineering the quantum-classical interface of solid-state qubits," *npj Quantum Information*, vol. 1, no. 1, p. 15011, 2015/10/27 2015, doi: 10.1038/npjqi.2015.11.

[21] M. C. Hamilton, B. Yelamanchili, A. Shah, S. E. Peek, S. Bankson, and C. C. Tillman, "Superconducting Microwave Interconnect Technologies for Quantum and Cryogenic Systems," in *2022 IEEE/MTT-S International Microwave Symposium - IMS 2022*, 19-24 June 2022 2022, pp. 72-75, doi: 10.1109/IMS37962.2022.9865377.

[22] D. Awschalom *et al.*, "Development of Quantum Interconnects (QuICs) for Next-Generation Information Technologies," *PRX Quantum*, vol. 2, no. 1, p. 017002, 02/24/ 2021, doi: 10.1103/PRXQuantum.2.017002.

[23] B. Yelamanchili *et al.*, "Face-to-Face Cable Interconnect Scheme for Thin Flexible Superconducting Stripline Cables," *IEEE Transactions on Applied Superconductivity*, vol. 32, no. 4, pp. 1-5, 2022, doi: 10.1109/TASC.2022.3149729.

[24] K. Kang *et al.*, "A 5.5mW/Channel 2-to-7 GHz Frequency Synthesizable Qubit-Controlling Cryogenic Pulse Modulator for Scalable Quantum Computers," in *2021 Symposium on VLSI Circuits*, 13-19 June 2021 2021, pp. 1-2, doi: 10.23919/VLSICircuits52068.2021.9492343.

[25] M. Stanley, S. D. Graaf, T. Hönigl-Decrinis, T. Lindström, and N. M. Ridler, "Characterizing Scattering Parameters of Superconducting Quantum Integrated Circuits at Milli-Kelvin Temperatures," *IEEE Access*, vol. 10, pp. 43376-43386, 2022, doi: 10.1109/ACCESS.2022.3169787.

[26] M. Stanley, R. Parker-Jervis, S. de Graaf, T. Lindström, J. E. Cunningham, and N. M. Ridler, "Validating S-parameter measurements of RF integrated circuits at milli-Kelvin temperatures," *Electronics Letters*, https://doi.org/10.1049/ell2.12545 vol. 58, no. 16, pp. 614-616, 2022/08/01 2022, doi: https://doi.org/10.1049/ell2.12545.

[27] J. M. Kast, P. Manurkar, K. Remley, R. D. Horansky, and D. Williams, "Traceable mmWave Modulated-Signal Measurements for OTA Test," presented at the 99th ARFTG Microwave Measurements Conference, Denver, 2022.

[28] P. Rabl, D. DeMille, J. M. Doyle, M. D. Lukin, R. J. Schoelkopf, and P. Zoller, "Hybrid Quantum Processors: Molecular Ensembles as Quantum Memory for Solid State Circuits," *Physical Review Letters*, vol. 97, no. 3, p. 033003, 07/21/ 2006, doi: 10.1103/PhysRevLett.97.033003.

[29] D. Nghiem, J. T. Williams, and D. R. Jackson, "A general analysis of propagation along multiple-layer superconducting stripline and microstrip transmission lines," *IEEE Transactions on Microwave Theory and Techniques*, vol. 39, no. 9, pp. 1553-1565, 1991, doi: 10.1109/22.83831.

[30] P. Duthil, "Material Properties at Low Temperature," in *CAS-CERN Accelerator School: Superconductivity for Accelerators*, R. Bailey Ed. Erice, Italy, 2013.

[31] J. V. Butler, D. Rytting, M. F. Iskander, R. D. Pollard, and M. Vanden Bossche, "16-term error model and calibration procedure for on-wafer network analysis measurements," *IEEE Trans. Microw. Theory Techn.*, vol. 39, no. 12, pp. 2211-2217, December 1991.

[32] J. A. Jargon, D. F. Williams, and A. Sanders, "The Relationship Between Switch-Term-Corrected Scattering-Parameters and Wave-Parameters Measured With a Two-Port Vector Network Analyzer," *IEEE Microw. Wireless Comp. Lett.*, vol. 28, no. 10, pp. 951-953, 2018, doi: 10.1109/LMWC.2018.2867076.

[33] R. B. Marks and D. F. Williams, "A general waveguide circuit theory," *J. Res. Nat. Instit. Standards Technol.*, vol. 97, no. 5, pp. 533-562, September 1992.

[34] D. F. Williams and B. Alpert, "Causality and waveguide circuit theory," *IEEE Trans. Microw. Theory Techn.*, vol. 49, no. 4, pp. 615-623, 4/1/2001 2001.

[35] J. Verspecht, F. Verbeyst, and M. Vanden Bossche, "Network Analysis Beyond S-parameters: Characterizing and Modeling Component Behaviour under Modulated Large-Signal Operating Conditions," presented at the ARFTG Microw. Meas. Conf., 4/2009, 2009.

[36] *NIST Microwave Uncertainty Framework*. (2011). National Institute of Standards and Technology, http://www.nist.gov/ctl/rf-technology/related-software.cfm. [Online]. Available: http://www.nist.gov/ctl/rf-technology/related-software.cfm

[37] S. Vandenplas, J. Verspecht, F. Verbeyst, E. Vandamme, and M. Vanden Bossche, "Calibration issues for the large signal network analyzer (LSNA)," presented at the ARFTG Microw. Meas. Conf., 12/5/2002, 2002.

[38] P. D. Hale *et al.*, "Traceability of high-speed electrical waveforms at NIST, NPL, and PTB," in *Conf. Precision Electromagn. Meas.*, 1-6 July 2012, pp. 522-523, doi: 10.1109/CPEM.2012.6251033.

[39] A. Ferrero, "Two-port network analyzer calibration using an unknown 'thru'," *IEEE Microw. Guided Wave Lett.*, vol. 2, no. 12, pp. 505-507, 1992.
[40] R. E. Collin, *Foundations for Microwave Engineering*. McGraw-Hill, Inc., 1966.
[41] R. B. Marks, "A multi-line method of network analyzer calibration," *IEEE Trans. Microw. Theory Techn.*, vol. 39, no. 7, pp. 1205-1215, July 1991.
[42] R. B. Marks and D. F. Williams, "Characteristic Impedance Determination using Propagation Constant Measurement," *IEEE Microw. Guided Wave Lett.*, vol. 1, no. 6, pp. 141-143, June 1991.
[43] D. F. Williams and R. B. Marks, "Transmission Line Capacitance Measurement," *IEEE Microw. Guided Wave Lett.*, vol. 1, no. 9, pp. 243-245, September 1991.
[44] M. Schroeder, "Synthesis of low-peak-factor signals and binary sequences with low autocorrelation (Corresp.)," *IEEE Trans. Information Theory*, vol. 16, no. 1, pp. 85-89, 1970, doi: 10.1109/TIT.1970.1054411.
[45] A. Sanders, D. Williams, J. M. Kast, K. Remley, and R. D. Horansky, "Large-Signal-Network-Analyzer Phase Calibration on an Arbitrary Grid," presented at the IEEE Int. Microw. Symp., Boston, MA, June 2-7, 2019.
[46] J. Verspecht, "Large-Signal Network Analysis," *IEEE Microw. Mag.*, vol. 6, no. 4, pp. 82-92, 12/2005 2005.

ELYSE MCENTEE WEI (Graduate Student Member, IEEE) graduated magna cum laude from Willamette University with her B.A in physics in 2010. She is a graduate student in the physics department at the Colorado School of Mines and is working towards her Ph.D. in collaboration with the National Institute of Standards and Technology as a GFSD/GMSE fellow. Elyse is a lifetime member of the Phi Beta Kappa honor society.

RICHARD A. CHAMBERLIN. Refugee from sub-mm radio astronomy now working in support of quantum computing.

NATE KILMER (Member, IEEE) received a B.S. in Electrical Engineering from the University of Colorado, Colorado Springs in 2019. After graduating, he was accepted into the Professional Research Experience Program where he worked with the High-Speed Measurements Group in the RF Technology Division at the National Institute of Standards and Technology. Upon completing his fellowship in the Professional Research Experience Program he accepted a position with Bold Renewables in Windsor, Colorado working with photovoltaic inverters. He is currently pursuing an M.E. at Colorado State University specializing in electric power and energy.

JOSHUA M. KAST (Student Member, IEEE) is a PhD candidate at Colorado School of Mines, Department of Electrical Engineering. He received his Bachelor of Science degree in Chemistry, and Master of Science degree in Electrical Engineering in 2011 and 2017 respectively, both from Colorado School of Mines. His current areas of research include computational electromagnetics with emphasis on the finite-difference time-domain method, and measurement of nonlinear microwave devices.

JAKE A. CONNORS received a Ph.D. in Physics from Harvard University in 2018, where he studied channel length scaling in microwave graphene field effect transistors. He was then a NASA Postdoctoral fellow at NASA Goddard Space Flight Center before coming to NIST in 2020, where he works on the development of ultra-low noise bolometers for applications in the microwave through far-infrared. He was recently named a NASA Nancy Grace Roman Technology Fellow for his work on ultra-low noise Far-Infrared Transition Edge Sensor Bolometers.

DYLAN WILLIAMS (Life Fellow, IEEE) received a Ph.D. in Electrical Engineering from the University of California, Berkeley in 1986. He joined the Electromagnetic Fields Division of the National Institute of Standards and Technology in 1989 where he develops electrical waveform and microwave metrology. He has published over 140 technical papers and is a Fellow of the IEEE. He is the recipient of the Department of Commerce Bronze and Silver Medals, the Astin Measurement Science Award, two Electrical Engineering Laboratory's Outstanding Paper Awards, three Automatic RF Techniques Group (ARFTG) Best Paper Awards, the ARFTG Automated Measurements Technology Award, the IEEE Morris E. Leeds Award, the European Microwave Prize and the 2013 IEEE Joseph F. Keithley Award. Dylan also served as Editor of the IEEE Transactions on Microwave Theory and Techniques from 2006 to 2010, as the Executive Editor of the IEEE Transactions on Terahertz Science and Technology, and as the 2017 President of the IEEE Microwave Theory and Techniques Society.